16th World Conference on Earthquake, 16WCEE 2017

Santiago Chile, January 9th to 13th 2017

Paper N° 3999

Registration Code: S-Q1467291768

ANALYSIS OF FULL-SCALE BUILDING COLLAPSE TEST USING FIBER HINGE ELEMENT CONSIDERING TWO-DIRECTIONAL COLUMN DETERIORATIONS

K. Kasai[1], TT. Nam[2]

[1] *Professor, Tokyo Institute of Technology, kasai@serc.titech.ac.jp*
[2] *Lecturer, Ho Chi Minh City University of Architecture, tuanam@yahoo.com*

Abstract

A full-scale four-story steel building specimen was experimented using the E-Defense shake table in 2007, wherein various increasing scaled ground motions were applied until collapse. As a part of the investigation on the building response, this paper addresses the deterioration of the column subjected to simultaneous biaxial moment and axial force, which caused local buckling, consequent decrease in base shear capacity, and eventual structural collapse.

Experimental results show totally different deteriorating patterns of biaxial bending moments among all six columns because their axial force magnitudes differ considerably due to the column locations. Shifting of the principal direction of the biaxial bending moments cycle by cycle also caused the initiating damage of column section in the X direction and consequently reducing the resistant capacity in the Y direction. The evolution of column deterioration is clarified and detailed from these perspectives.

The fiber hinge element that consists of fibers discretizing the column cross section is used to simulate the moment deterioration caused by local buckling. The parameters defining the fiber hinge element are determined from the behavior of the cantilever column tested using an identical steel member. The analysis using the fiber hinge element appears to simulate well the two-directional deterioration behavior under complex loading such as compression and tensile axial load applied alternately, additional high frequency axial load caused by vertical accelerations, and shifting of the principal directions of the bending moments cycle by cycle.

On the other hand, this study provides further interpretation of the building response in terms of energy, in which the energy input and the dissipation mechanism at the collapse excitation state are evaluated. Although the total accumulated input energies were very similar in both directions, the input energy in the X direction increased gradually, whereas the input energy in the Y direction had a suddenly large instantaneous amount needed to dissipate within a short time by the frame with limited strength due to deterioration, thereby resulting in the rapid translational response and collapse of the first story mainly in the Y direction.

Keywords: collapse experiment; column deterioration; varying axial load; local buckling; fiber hinge element

1. Introduction

A collapse experiment on a full-scale four-story steel building was conducted on the E-Defense shake-table facility located in Miki City, Hyogo Prefecture, Japan, in September 2007. It was a part of an experimental project on steel buildings conducted at the E-Defense shake table facility. An overview of the project was described in [1], whereas the collapse test and result are described in [2–4]. The three-directional ground acceleration histories recorded at the JR Takatori station during the 1995 Hyogo-ken Nanbu earthquake were used, by scaling the records by 0.05, 0.2, 0.4, 0.6, and 1.0 times. Collapse occurred at 1.0 times the acceleration (100% Takatori motion level) with a soft-story mechanism. The experiment attracted interest from research and practice communities in studying and establishing an effective model to simulate the collapse of the building specimen.

Two-dimensional (2D) numerical methods were adopted by several researchers. [5] and [6] closely simulated displacement histories in the longitudinal direction of the frame that developed the largest responses. Their approaches both considered column deterioration after buckling, but did not consider the reduction of yield moment capacity due to significantly varying axial force caused by the seismic building overturning moment. Detailed three-dimensional (3D) finite element models, therefore, would be more appropriate to analyze the test, and they were used by [7–9]. However, those simulations required large modeling and computational efforts, not really necessary for the most of structural components responding elastically or even inelastically as long as simpler analytical techniques are available.

This study utilizes a simplified analytical technique considering the so-called "*fiber hinge element*" to simulate steel column local buckling. Because the concentrations of plasticity and local buckling occur at the ends of frame members, the fiber hinge element is used only at the column ends, unlike the fiber beam element approach [9] discretizing the column section throughout the member length. The fiber hinge element has zero length but considers a yield-zone length for the fiber to simulate elastoplastic and local buckling behaviors. Other portions of the frame are modeled by the beam, truss, and spring elements.

The main objective of this paper is to clarify two-directional column behavior and deteriorations, as well as consequent collapse of the full-scale four-story steel building via analyses utilizing the fiber hinge elements. The columns were under varying axial load and biaxial bending moment, deteriorating due to local buckling, and causing three-dimensional collapse of the building. Accuracy of the analysis method is demonstrated via nonlinear dynamic analyses of the isolated column element as well as the entire four-story building. Moreover, this study provides further interpretation of the building response in terms of energy, in which the energy input and the dissipation mechanism at the collapse excitation state are evaluated. Although the total accumulated input energies were very similar in both directions, the input energy in the X direction increased gradually, whereas the input energy in the Y direction had a suddenly large instantaneous amount needed to dissipate within a short time by the frame with limited strength due to deterioration, thereby resulting in the rapid translational response and collapse of the first story mainly in the Y direction.

2. Full-scale 4-story steel building collapse test

2.1 Building specimen and input ground motion

The building specimen [Fig.1(a)] is a full-scale four-story steel moment frame whose plan dimension is 6 ×10 m [Fig.1(b)], and the height is 14.375 m [Fig.1(c)]. The total weight from mid-height of the first-story level column to the top of the building is 2,019 kN. SN400B and BCR295 steel were used for the beams and columns, respectively. The section shapes are given in Table 1.

Autoclaved lightweight concrete (ALC) external cladding panels were placed on three sides of the structure. The columns are constructed using 300×300×9 cold-formed square tubes with relatively large width-to- thickness ratios (b/t = 33). The columns are welded to 50 mm thick baseplates (SN490C). Each baseplate is bolted using 8 anchor bolts of M36 (ABR490, 900 mm length) to fixtures attached to the shake-table. The beams are constructed using hot-rolled wide flanges. Welding details with no weld access hole, which were

Table 1 – Sections and materials of the steel frame

Beam (SN400B)				Column (BCR295)	
Floor	G1	G11	G12	Story	C1,C2
R	H-346×174×6×9	H-346×174×6×9	H-346×174×6×9	4	RHS-300×300×9
4	H-350×175×7×11	H-350×175×7×11	H-340×175×9×14	3	RHS-300×300×9
3	H-396×199×7×11	H-400×200×8×13	H-400×200×8×13	2	RHS-300×300×9
2	H-400×200×8×13	H-400×200×8×13	H-390×200×10×16	1	RHS-300×300×9

H- height × width × web thickness × flange thickness; RHS- height × width × thickness

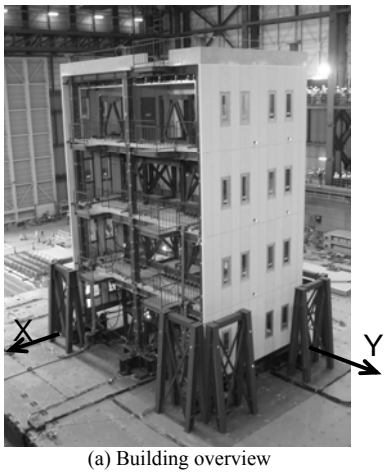

(a) Building overview

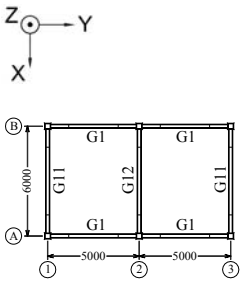

(b) Plan

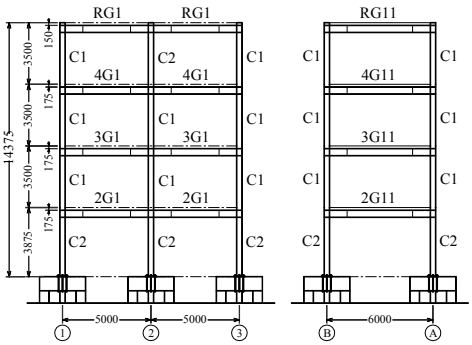

(c) Elevation

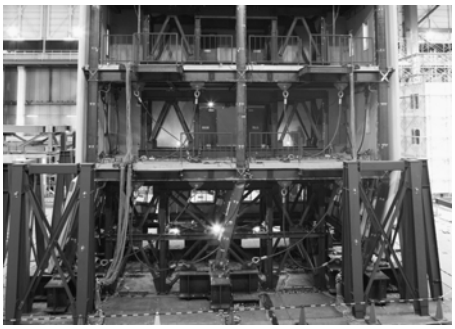
(d) Building collapse

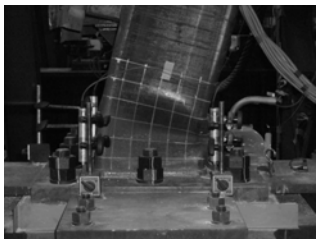
(e) Local buckling at column end

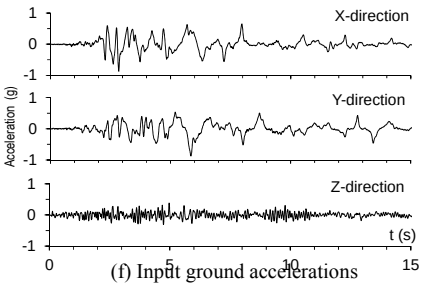

(f) Input ground accelerations

Fig.1 – Full-scale 4-story steel building specimen and input ground motion

recommended after the Kobe earthquake, are adopted for the beam-to-column connections. Fully composite action is expected between steel beams and concrete slab. Fig.1(d) shows the post-collapse configuration of the building with soft-story mechanism caused by deterioration of first-story columns due to local buckling at column ends [Fig.1(e)].

The ground acceleration histories recorded at the JR Takatori station during the 1995 Hyogo-ken Nanbu earthquake (herein referred to as Takatori motion) were used as the input for the shake table experiments. The building specimen was subjected to a series of white noise motions and progressively increasing scaled Takatori motion from 5 to 100%. The EW, NS, and UD components of the ground motion were considered for the X, Y, and Z directions, respectively [Fig.1(f)].

Sign conventions for lateral displacement (u_X, u_Y), story drift ratio (r_X, r_Y) and moment (M_Y, M_X) are presented in Fig.2(a)-right. Note that M_Y (moment about the Y axis) relates to r_X (lateral deformation along the X axis), whereas M_X (moment about the X axis) corresponds to r_Y (lateral deformation along the Y axis). Therefore in this study, positive M_X is exceptionally defined inverse to the right-hand rule, in order to present the proportionality of lateral deformation and consequent moment.

2.2 Accumulated two-directional column deterioration due to local buckling

The yield capacity is governed by axial force and biaxial moments. When the column yields, its moment capacity follows the yield surface. However, if local buckling occurs, the yield surface may shrink down and consequently reduces the moment capacity. Therefore, the study utilizes the existing equation of yield capacity as an indicator to detect the deterioration. Eq.(1) shows the *combined strength factor R* counting for the simultaneous interaction of axial force and biaxial moments for square tube columns, *i.e.*,

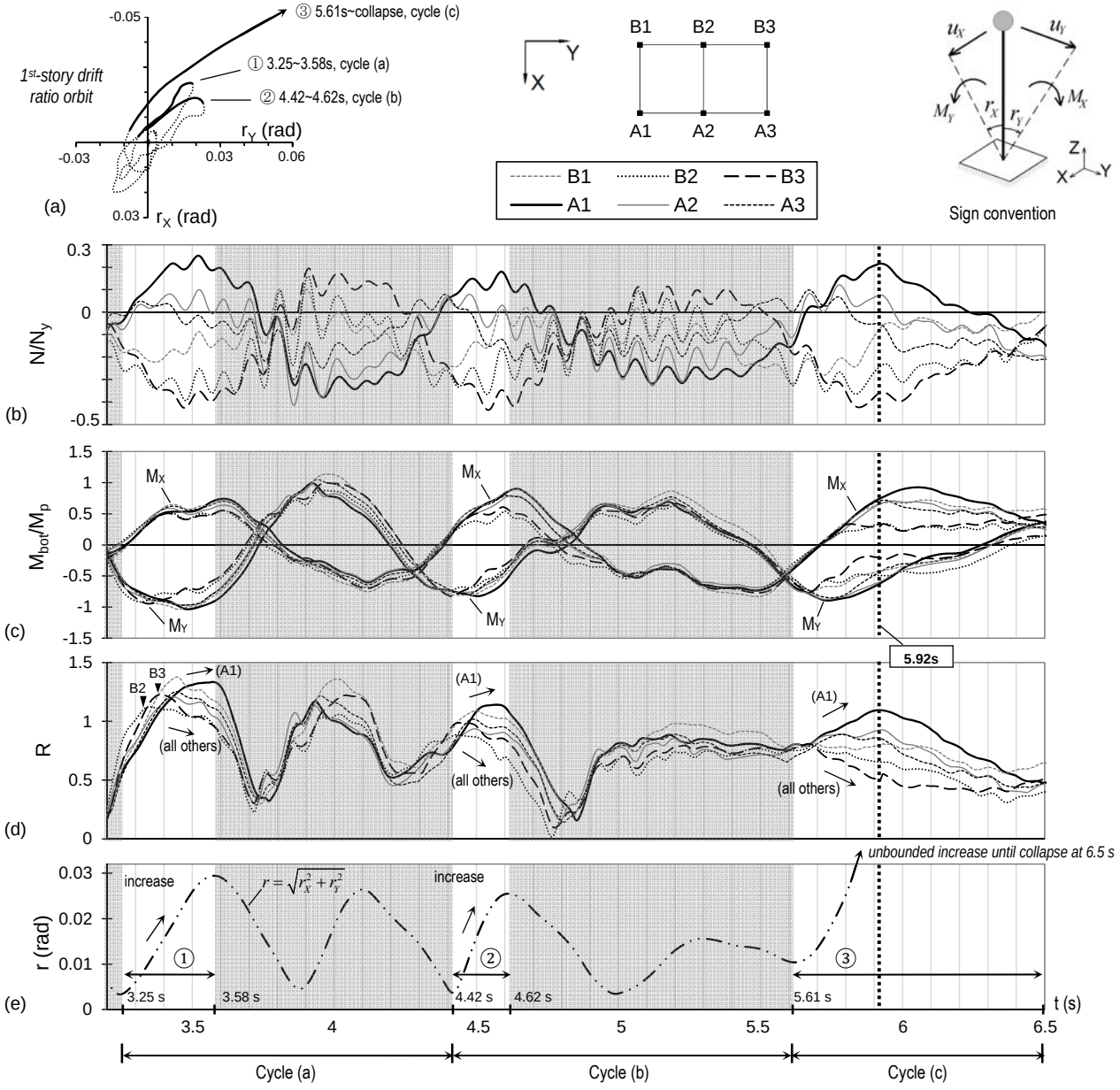

Fig. 2 – (a) 1st-story drift ratio orbit, and time histories of (b) axial forces, (c) bottom moments, (d) combined strength factor R of 1st-story columns, and (e) 1st-story drift ratio $r = \sqrt{r_X^2 + r_Y^2}$ (100% Takatori level)

$$R = \frac{4}{3}\left(\frac{N}{N_y}\right)^2 + \frac{\max\left(|M_X|, |M_Y|\right)}{M_p} + \frac{3}{4}\left[\frac{\min\left(|M_X|, |M_Y|\right)}{M_p}\right]^2 \qquad (N/N_y \le 0.5) \qquad (1)$$

where, M_p is plastic moment in case of zero axial force. According to Inoue [10], R = 1.0 indicates the interaction of N, M_Y, and M_X at the yield surface in the case of $|N/N_y| \le 0.5$, corresponding to the present case where N/N_y varied from +0.25 to –0.44. R in fact can be larger than 1.0 because of strain hardening effect. When yielding occurs, if N increases, then moment capacity decreases. On the other hand, based on the relationship

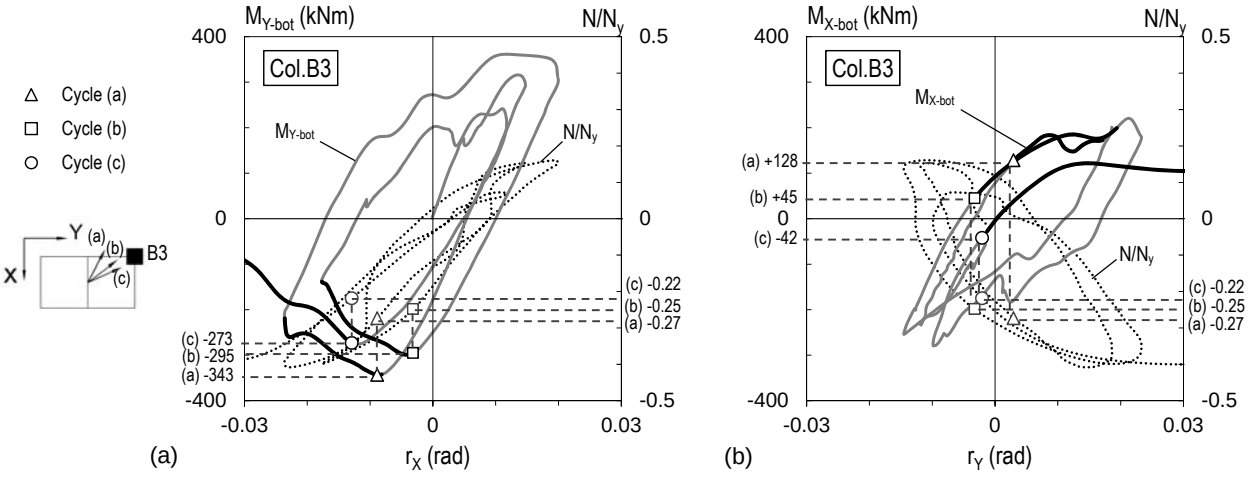

Fig. 3 – Column B3's bottom moment (*solid line*, primary axis) and low-pass filtered axial force (*dotted line*, secondary axis) vs. first-story drift ratio at 100% Takatori level, and moment and axial force magnitudes at three peaks of bottom moment ($M_{Y\text{-bot}}$) with compressive axial force condition.

between the development of R and the increase of story drift ratio in the radial direction $r = \sqrt{r_X^2 + r_Y^2}$, the judgment of column deterioration due to local buckling can be made whenever R reaches peak and then declines while $\dot{r} > 0$.

Fig.2 shows the (a) 1st-story drift ratio orbit, and time histories of (b) axial force including gravity load, (c) moment M_Y and M_X, (d) combined strength factor R of all six column bottom ends, and (e) 1st-story drift ratio r at 100% Takatori excitation level. Based on Fig.2(a), three main cycles are defined with durations of (a) 3.2~4.1 sec, (b) 4.2~5.0 sec, and (c) 5.6~6.5 sec, respectively. Each cycle is defined as the period whereby u_X makes a full loop from zero to zero. The cyclic change of displacement direction was shown, where the frame tended to yield toward the Y direction with the orientation angles of nearly 53°, 38°, and 29°, respectively in the sequence of three cycles. The Y direction was also the eventual collapse direction of the building in the cycle (c).

Three segments associated with the increasing progresses of r toward the $+r_Y$ direction at 100% Takatori level, denoted by ①, ②, and ③ [Fig.2(a)], are highlighted, and the other time zones are shaded. In the segment ① of cycle (a) when the r increased toward $+r_Y$ direction [Fig.2(e)], the reductions of factor R [Fig.2(d)] again occurred early to columns B2 and B3 at 3.33 sec and 3.37 sec, respectively, reflected mostly by the decrease of M_Y [Fig.2(c)]. The reductions of factor R occurred later to columns A2, A3 and B1, when r exceeded 0.02 rad. Column A1 was strongest during segment ① and almost did not show any deterioration, because it was under tension. A similar situation occurred in the subsequent segments ② and ③. Especially, although the magnitude of r remained almost similar after each cycle, the peak values of factor R gradually declined, indicating the cumulative deterioration caused by local buckling.

Fig.3 shows the hysteretic curves of the column B3's bottom moments $M_{Y\text{-bot}}$ and $M_{X\text{-bot}}$ at 100% Takatori motion level. The low-pass filtered version of column axial force (*dotted line*, in respect to secondary vertical axis) is also displayed in the plot, thereby showing the deterioration of $M_{Y\text{-bot}}$ mainly occurring under compressive load condition when the building deformed in the negative r_X direction. Note that the axial force is low-pass filtered to eliminate the high-frequency fluctuation due to vertical acceleration, in order to provide an easily identified hysteretic curve in Fig.3. Three points of timing when $M_{Y\text{-bot}}$ started decreasing due to local buckling: 3.35 sec (marked by Δ), 4.40 sec (□), and 5.68 sec (○) at three cycles (a), (b), and (c), respectively are therefore selected to show; and both moments and axial forces at those instants are also indicated in Fig.3. Because the principal direction of biaxial bending moment in cycle (a) was close to the X direction, $M_{Y\text{-bot}}$ early reached to peak capacity and then deteriorated due to local buckling. $M_{X\text{-bot}}$ developed later but could not achieve

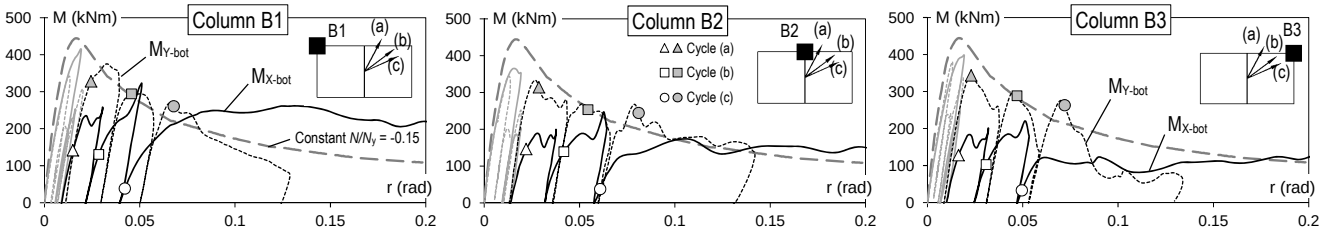

Fig. 4 – Accumulated deterioration of bottom moments of three selected columns B1, B2 and B3 characterized by skeleton curves for the negative $M_{Y\text{-bot}}$ and positive $M_{X\text{-bot}}$, with symbols commonly showing both values at the times of 3.35s, 4.43s and 5.73s of three cycles (a), (b) and (c), respectively.

high capacity as well as linear relation with the increasing story drift r_Y because of the damage by local buckling. Similar situations repeated in the subsequent cycles (b) and (c). In overall, the column was subjected to quite large compressive force of approximately $-0.25N_y$ when the local buckling and deterioration of $M_{Y\text{-bot}}$ started occurring.

The influence of compression force magnitude on the column moment deterioration is presented in the followings. Three columns having different levels of axial force variations excluding the high-frequency fluctuation: B1 (N/N_y varied from –0.2 to +0.0, *small compression*), B2 ($N/N_y \approx$ –0.3 to +0.1, *moderate compression*) and B3 ($N/N_y \approx$ –0.4 to +0.2, *large compression*) are selected to demonstrate. Fig.4 displays the accumulated moment deterioration of those columns presented in terms of skeleton curves whose plotting method is adopted from [11] can indicate the cyclic degradation of column moment due to local buckling. The symbols showing the timing points of three cycles are also plotted in Fig.4, indicating the earlier magnitude development of $M_{Y\text{-bot}}$ *(dashed line)* than $M_{X\text{-bot}}$ *(solid line)* within each cycle and consequent deterioration of $M_{X\text{-bot}}$ due to the preceding degraded $M_{Y\text{-bot}}$. On the other hand, the tangent stiffnesses at the early stage of $M_{X\text{-bot}}$ during each cycle were reduced to approximately 1/2 ~ 1/3 times those of $M_{Y\text{-bot}}$, confirming the two-directional correlative moment deterioration.

In addition, the skeleton curve by the cyclic bending test conducted prior to the collapse experiment (using the same column type under constant compression load of $-0.15N_y$) is included in Fig.4. Based on that, the difference of moment deteriorations among the three columns is easily recognized. The level of $M_{X\text{-bot}}$ deterioration increases from columns B1, B2 to B3. This is closely related to the different compression force magnitude that developed in the columns, as indicated earlier. Larger compression forces resulted in the more significant column deterioration. Hence, the $M_{X\text{-bot}}$ skeleton curve of column B3 during cycle (c) was much lower, whereas the one of column B2 was almost similar, and the one of column B1 was much higher than the one by component test (with constant $N/N_y = -0.15$).

3. Dynamic analyses of biaxial column bending with varying axial load

3.1 Concept of simulating local buckling by fiber hinge element

The buckling zone at the column ends [Fig.5(a)] is modeled as a fiber hinge element composed of tiny struts that can deteriorate due to buckling effect, namely fibers, discretizing the cross section [Fig.5(b)]. The hinge zone conveniently has zero length, unlike the other fiber beam element approach requiring mesh generation for expected yield zone length. Its rotation characteristic is achieved by its presumed finite length l_h of buckling zone. For the present tube column, l_h is set equal to the column depth based on the observations from experiment. The nonlinear stress-strain properties of the fiber element [Fig.5(c)] are stipulated by this finite length The degradation rule for the compressive buckling zone is specified by considering Yamada *et al.*'s [12] axial stress-strain rule constructed from pure compression tests of stub columns with *b/t* ratios varying from 15 to 35. As shown by Fig.5(d), the rule was utilized for initial setting of the fiber model for the present column section (*b/t* = 33).

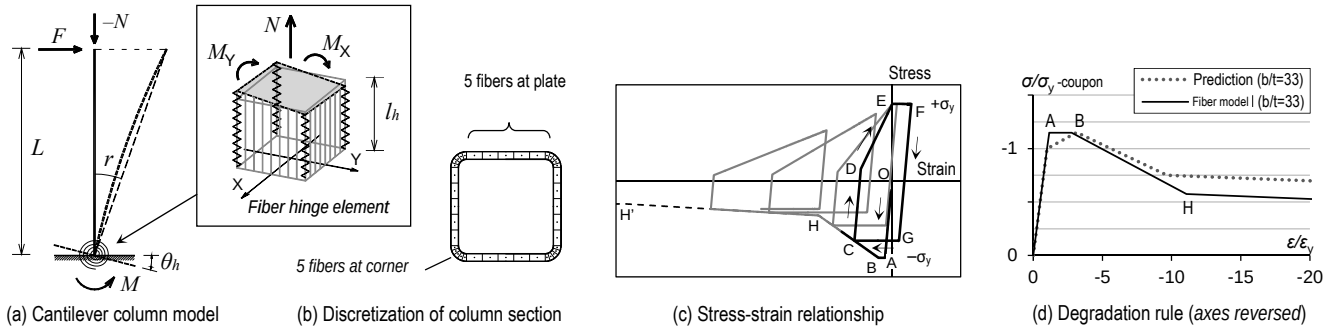

(a) Cantilever column model (b) Discretization of column section (c) Stress-strain relationship (d) Degradation rule (*axes reversed*)

Fig. 5 – Structural model, discretization scheme, and stress-strain property of fiber hinge element

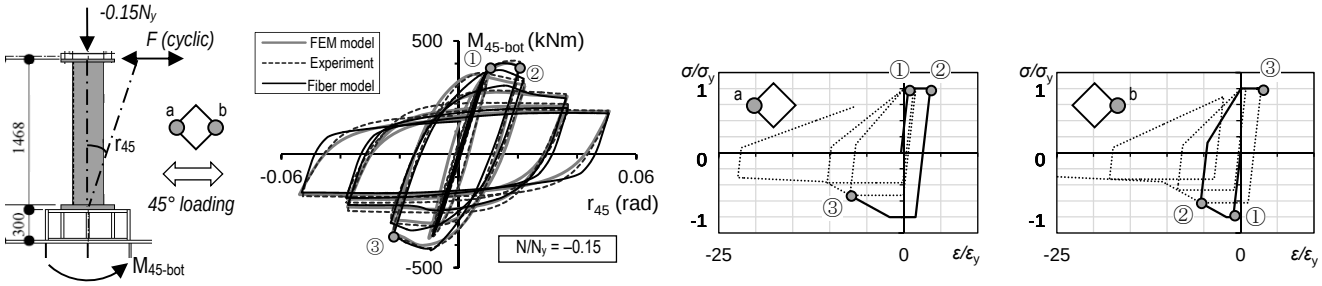

(a) Test setup (b) Column moment-rotation hysteresis (c) Stress-strain relation of fiber "a" (d) Stress-strain relation of fiber "b"

Fig. 6 – Simulation results for cyclic bending test of cantilever column, and stress-strain relationships of two selected fibers in fiber hinge model.

The result of simulation using fiber hinge element is validated by the cyclic bending test conducted prior to the collapse experiment [Fig.6(a)]. The cantilever column RHS-300×300×9 (identical to the member in the test building) was subjected to cyclic bending and constant compressive force of –500 kN (approximately –0.15N_y). Fig.6(b) plots the column moment- rotation relationship, showing the agreement between the simulation by *fiber model* with the experimental record. Fig.6(b) also includes simulation result by another analytical model using finite element method (noted as *FEM model*).

In order to produce similar deterioration of experimental column moment, parameter calibration is conducted for the model. Stress-strain relationships of two fibers "*a*" and "*b*" [Figs.6(c)–(d), respectively] located at opposite corners, showing completely different conditions under 45° cyclic bending, are used to illustrate the parameter calibration. Three points ①, ② and ③ shown in those graphs are related to those appeared in Fig.6(b). Upon point ①, fibers "*a*" and "*b*" start tensile and compressive yieldings, respectively. During the yielding until the unloading point ②, the buckling of fiber "*b*" [Fig.6(d)] is modeled to start at compressive strain of approximately 2.5ε_y [point B, Fig.5(c)] where ε_y is yield strain, and then starts degradation. Moment deterioration in the consecutive half cycle up to the next unloading point ③ is captured by the degradation of fiber "*a*" [Fig.6(c)] which is subsequently under compression. The stress of the buckled fiber beyond compressive strain of 10ε_y [point H, Fig.5(c)] is set to remain as 0.5σ_y, slightly modified from the prediction rule [Fig.5(d)] in order to simulate more closely the experimental cyclic degradation of column moment.

3.2 Analysis results for particular columns

This section presents a series of hypothetical time-history bending analyses using fiber hinge element conducted for three selected columns (B1, B2 and B3) in the first story level of the building. Assuming the inflection point remains stable at the middle height of the column, the analytical column models are constructed as cantilever columns with the height of $L = H/2 = 1750$ mm, where H is the actual first-story column height in the test frame.

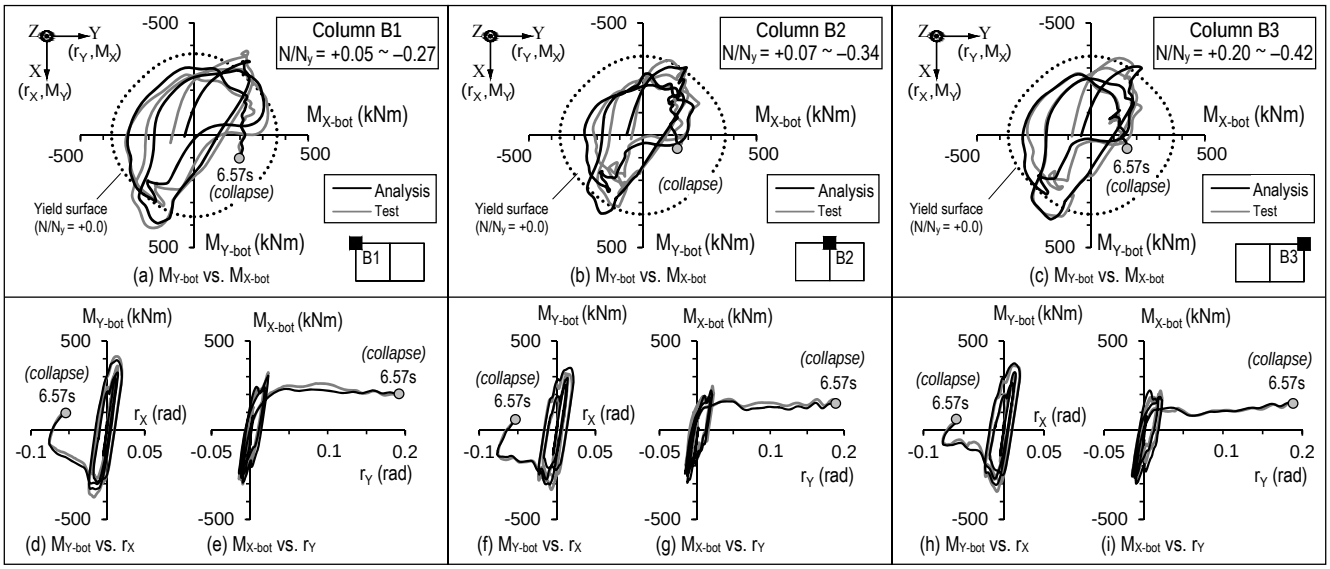

Fig. 7 – Analysis results of isolated columns, applying axial force and displacement histories by 100% Takatori

Displacement control is applied to the cantilever column model, wherein the tip end is subjected to the bi-directional lateral displacement history so as to reproduce the identical chord rotation as the first-story drift ratio recorded in the collapse test at 100% Takatori motion level [Fig.2(a)]. In addition, the experimental varying axial force histories (including gravity load and high-frequency fluctuation due to vertical accelerations) of each particular column recorded in the collapse test are also applied to the related column model.

Fig.7 shows good agreement between the analytical results and the experimental records. Three groups of graphs related to three columns with different varying levels of axial force: B1 (N/N_y varied from +0.05 to –0.27, *small compression*), B2 ($N/N_y \approx$ +0.07 to –0.34, *moderate compression*) and B3 ($N/N_y \approx$ +0.20 to –0.42, *large compression*) are shown respectively from left to right in Fig.7. Within each group, the upper graph plots the interacting relation between $M_{X\text{-bot}}$ (horizontal axis, related to r_Y) and $M_{Y\text{-bot}}$ (vertical axis, related to r_X) as well as the yield surface calculated from yield stress represented by dotted line. Note that the vertical axis is also reversed to define the moment coordinates consistent with the displacement coordinates presented earlier. The two lower graphs in each group show the hysteretic relationships "$M_{Y\text{-bot}}$ vs. r_X" and "$M_{X\text{-bot}}$ vs. r_Y" from left to right, respectively. Furthermore, to clarify the moment interaction surface, the curves relating to the elastic loading time before 3.2 sec [*i.e.* the start of the first cycle (a)] are omitted. The stop point marked by circle symbol is related to 6.57 sec, the time when the building completely collapsed and settled on the supporting safeguard system.

During the first two cycles of loading close to the r_X direction, $M_{Y\text{-bot}}$ developed earlier than $M_{X\text{-bot}}$ and rapidly reached to yield surface. However, the difference of axial force variation caused different responses of $M_{Y\text{-bot}}$ among the three columns during this time. $M_{Y\text{-bot}}$ of column B1 which had the smallest compression force hence was quite stable on both $-r_X$ and $+r_X$ loading directions [Fig.7(d)]. In contrast, the $M_{Y\text{-bot}}$ capacity of columns B2 [Fig.7(f)] and B3 [Fig.7(h)] was reduced significantly, especially on the $-r_X$ side, where they were carrying quite large compression forces. Local buckling must have occurred considerably to those columns during this time, thereby limiting their moment capacity. Consequently, the development of $M_{X\text{-bot}}$ was limited, particularly in the last half cycle until collapse at nearly 0.2 rad of r_Y deformation. Three increasingly significant levels of $M_{X\text{-bot}}$ deterioration during that time (characterized by the decreasing ratio of the average remaining capacity to the nominal plastic moment M_p) are easily recognizable from columns B1 [Fig.7(e), ratio 0.67] to B2 [Fig.7(g), ratio 0.48] and B3 [Fig.7(i), ratio 0.31]. The moment interaction surface of column B1 [Fig.7(a)] appeared to be strongest among the three columns, whereas the ones of columns B2 [Fig.7(b)] and B3 [Fig.7(c)] were much more shrinking, especially near the collapse time.

3.3 Simulation of building collapse using fiber hinge element

The building specimen is three-dimensionally modeled with the fiber hinge element applied for modeling the column ends. Fig.8 displays the analysis results of displacement for the collapse excitation (100% Takatori level) in terms of 1st story drift ratio orbit [Fig.8(a)] and time-histories of r_X and r_Y [Figs.8(b)–(c), respectively], showing good agreement with those recorded in the test. Note that the model was subjected to the 60–100% Takatori consecutive input motions to reflect the cumulative yielding and deterioration of structure. Fig.8(d) presents the motion trajectories of the entire system including shake table and all stories during the time from 5.5 to 6.5 sec in the last half cycle (c). The broken line stands for the shake table motion. From inside to outside, the solid lines indicate absolute displacements of the first-, second-, third-story and roof levels. The story-drift velocity can be estimated based on the 0.1-sec increments marked by circles on the displacement orbit. The sudden increase in deformation at the first story during this time was well simulated by the analytical model (represented by the black thin lines with floor symbols) in comparison with experimental records (gray thick line without floor symbols).

The agreement between analytical results and experimental records can be shown by not only the plan but also the elevation view of floor absolute displacement. Along the X direction [Fig.8(e)], the deformation magnitude increased nonlinearly at the first story from 5.9 sec. The response velocity of the first story was smaller than the input ground velocity, and the structure was shaken suddenly. Moreover, shaking action is more apparent in the Y direction [Fig.8(f)] from 5.9 to 6.2 sec, where the shake table already had reversed motion but the first story still kept moving forward, as indicated by the opposite arrows in the figure. The soft-story collapse mechanism induced by column deterioration was formally initiated at approximately 5.9 sec in the Y direction. Deformations then progressively concentrated in the first story until collapse because it experienced softening.

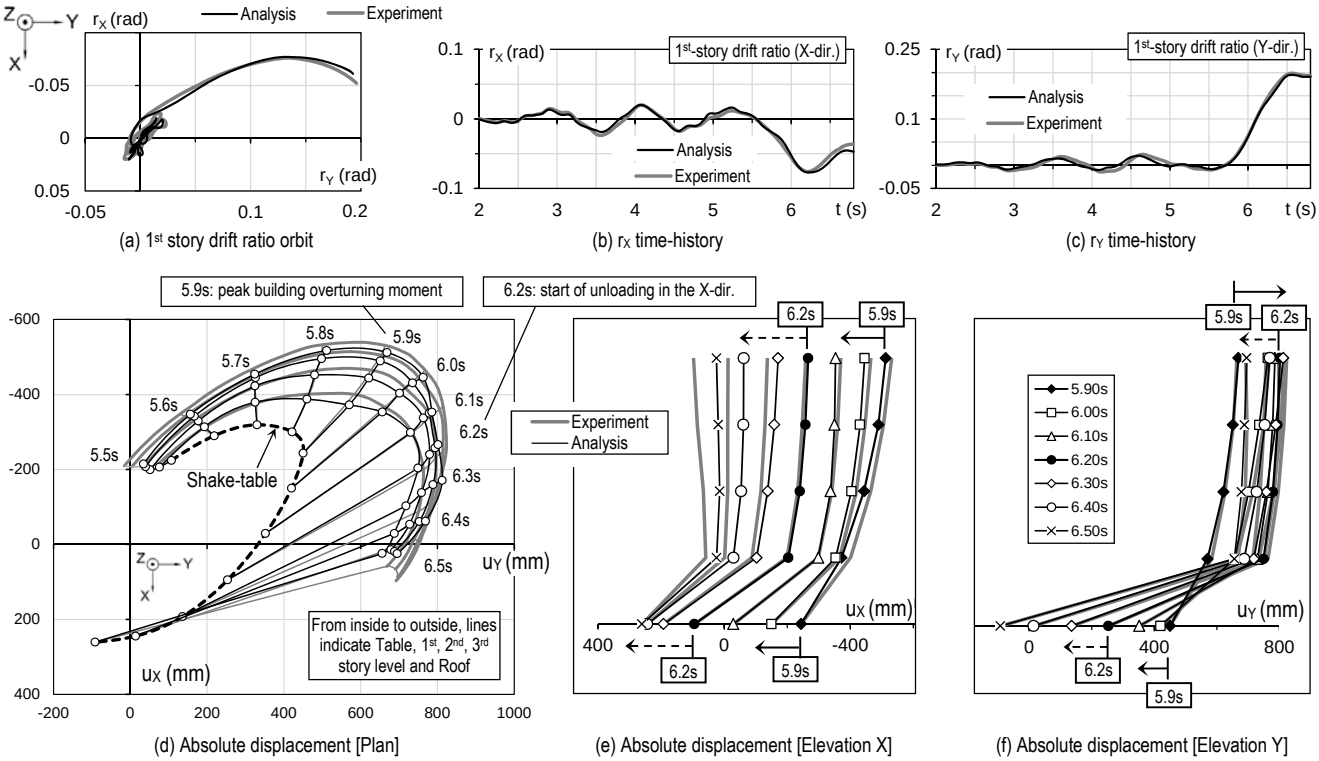

Fig. 8 – Analysis results of 1st story drift ratio orbit and time histories, and absolute displacement of the building and shake-table at 0.1-sec increments (100% Takatori level, 5.5~6.5 sec)

4. Energy input and dissipation at various shaking levels

4.1 Earthquake input energy

The earthquake input energy E_{in} (in either the X or Y direction) is calculated using the following equation, where m_i and $\dot{u}_i$ represent the lumped mass and the relative velocity of the i^{th} floor with respect to the shake table, respectively; n is the number of stories; and $\ddot{u}_g$ is the shake table input acceleration:

$$E_{in} = -\int \sum_{i=1}^{n} \dot{u}_i m_i \ddot{u}_g dt \tag{2}$$

Note that the energy in the equation is the relative energy based on the relative velocity and displacement between the structure and the ground (or shake table). The input and response energy quantities for 40, 60, and 100% Takatori motion levels are scaled to 20% Takatori motion for direct comparison (Fig.9) using the scale factor α = 1/2, 1/3, and 1/5, respectively. As indicated by Eq.(2), because there are two time-dependent quantities, i.e., the input ground acceleration $\ddot{u}_g(t)$ and the i^{th}-floor response velocity $\dot{u}_i(t)$, the scaled earthquake input energy $\alpha^2 E_{in}$ is used in the graphical presentation in Figs.9(a)–(b) for the X and Y directions. Up to 40% Takatori level, $\alpha^2 E_{in}$ during the cycles (a) and (b) was similar for all levels for both the X and Y directions. As yielding occurred, especially at the 100% Takatori level, $\alpha^2 E_{in}$ started to increase to nearly twice the values at previous levels. However, at each shaking level, the input energy in the X direction during these two cycles was approximately two to three times the input energy in the Y direction due to the stronger ground motion as well as larger response.

The instantaneous input energy, defined as dE_{in}/dt, in the X direction [Fig.9(c)] was also very high during the first two main cycles and much larger than that in the Y direction [Fig.9(d)]. Moreover, from 5.7 to 6.0 sec,

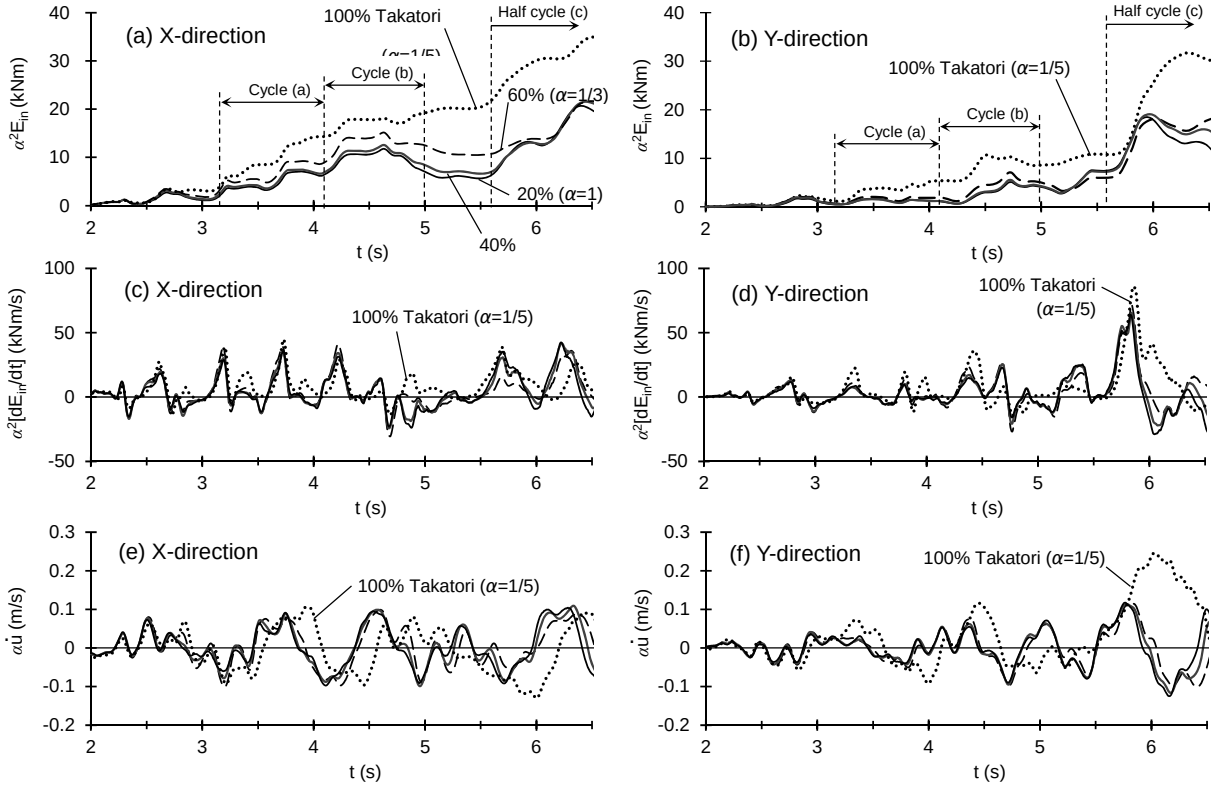

Fig. 9 – Time histories of normalized (a),(b) input energy, (c),(d) instantaneous input energy, and (e),(f) first-story relative velocity: scale factor α = 1, 1/2, 1/3 and 1/5 for 20, 40, 60 and 100% Takatori levels, respectively.

dE_{in}/dt in the Y direction increased to a remarkable peak [Fig.9(d)] and was similar for all excitation levels. As a result, $\alpha^2 E_{in}$ in the Y direction rapidly increased during this shaking period [Fig.9(b)], thereby causing greater dissipation demand in the frame and consequently very large displacements due to the deteriorated strength in the Y direction. Figs.9(a)–(b) also show that $\alpha^2 E_{in}$ at collapse (and at the end) are similar for the X and Y directions, thus suggesting that the above behavior cannot be predicted by such total input energy.

4.2 Energy dissipation at the collapse excitation level

The building response during the half cycle (c) at the 100% Takatori level can be interpreted using energy equilibrium. Because the 100% Takatori motion is 1.66 times greater than the 60% Takatori motion, its input energy should be $1.66^2 = 2.76$ times greater if the structure is elastic [see Eq.(2)].

Figs.10(a)–(b) show the hysteretic relationship between the *base shear* $Q_{acc,Y}$ (based on floor inertial forces obtained from floor accelerations) and the *first-story drift ratio* r_Y within the half cycle (c) for the 60 and 100% Takatori levels, respectively. For the 100% Takatori level, because of the limited strength due to deterioration and the P-Δ effect, the hysteretic branch greatly extended to dissipate the vertical striped area ΔE_{100} [Fig.10(b)] of 2.76 times the area ΔE_{60} [Fig.10(a)] enclosed by the 60% Takatori level from 5.7 to 6.0 sec. The dissipation of ΔE_{100} was finished even before 6.0 sec (i.e. 5.97 sec) because of the structural yielding. In other words, within such a short time, the story drift r_Y had to quickly increase from zero to 0.064 rad (100% Takatori level) which is much greater than 0.019 rad (60% Takatori level). This explains the bifurcation of the *relative story velocity* $\dot{u}_Y$ history at the 100% Takatori level [Fig.9(f)] at 5.7 sec, causing its response to be completely different from those for previous motion levels.

However, because the exceedingly large amount of instantaneous input energy in the Y direction needed to dissipate within a short time, the peak $\dot{u}_Y$ at 6.0 sec [Fig.9(f)] was more than twice that of $\dot{u}_X$ [Fig.9(e)]. Consequently, the building rapidly translated and collapsed in the Y direction, although the total input energies in the X and Y directions were nearly equal [Figs.9(a)–(b), respectively]. Therefore, this is an important issue in evaluating and predicting the vulnerable side of the building displacement response; *maximum instantaneous input energy* is thought to play a more important role than does *total input energy* in determining the main response of the structure. Fig.10(c) plots the breakdowns of accumulated energy distribution per story in the building in the X and Y directions, at three selected times of three cycles. From bottom to top, the levels indicate the energy dissipation by the first, second, third and fourth stories. The energy dissipation was dominant in the first story, indicating the significant yielding activity in this story level. On the other hand, because the earthquake input energy was larger in the X direction than in the Y direction during the first two cycles (a) and (b), the energy dissipation was also more dominant in the X direction than in the Y direction. However, with the sudden increase of earthquake input energy in the Y direction during the last cycle (c), the rapidly dissipated energy was mostly concentrated in the first story causing the soft-story collapse mechanism in the Y direction.

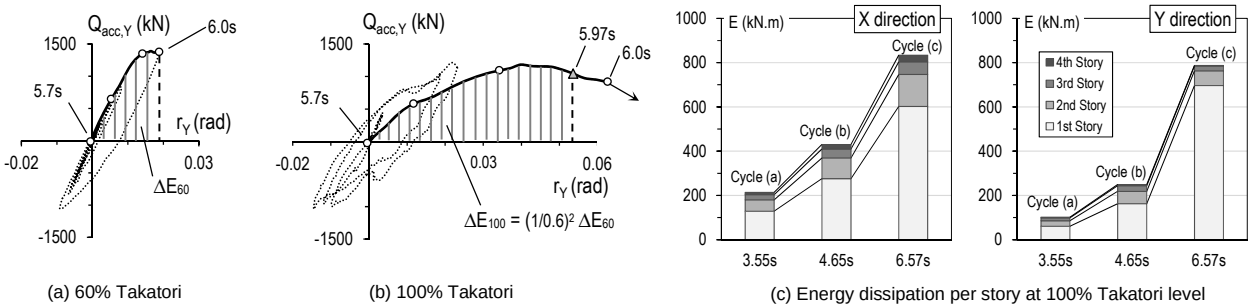

(a) 60% Takatori (b) 100% Takatori (c) Energy dissipation per story at 100% Takatori level

Fig. 10 – Hysteretic graphs characterizing the energy dissipation demand of the first story within the time from 5.7 to 6.0 sec in the Y direction, at (a) 60% and (b) 100% Takatori levels; and (c) accumulated energy dissipation per story at three points of time in three main cycles during the 100% Takatori loading.

5. Conclusions

- The interaction between axial force and two-directional moment deterioration observed in the full-scale building collapse test was indicated in this study. The fiber hinge element used to model the buckling zone at the column end proved its advantage in the analyses. Dynamic simulations of isolated particular cantilever columns applying the collapse experimental histories of two-directional lateral displacements and varying axial forces shows the efficiency of fiber hinge element method in simulating the column response under sophisticated axial load conditions.

- Due to the effects of complex loading such as alternately applied compressive and tensile axial load, additional high frequency axial load induced by vertical accelerations, and shifting of the principal directions of the bending moments cycle by cycle, a three-dimensional analytical model proves its appropriateness in simulating the building response in this collapse test.

- The sudden increase in the damage in the Y direction could be explained based on input energy, which depends on not only ground motion but also response velocity. Although the total accumulated input energies were very similar in both the X and Y directions, a large amount of instantaneous input energy in the Y direction had to be dissipated within a short time by the frame with limited strength due to deterioration, thereby resulting in the rapid translational response of the first story. Therefore, the maximum instantaneous earthquake input energy should be of greater interest in predicting structural response in seismic design.

Acknowledgements

This study is a part of "NEES/E-Defense collaborative research program on steel structures", and the team leader for the overall program is Prof. Kazuhiko Kasai (Tokyo Institute of Technology, Japan). The tests described in this paper were pursued by the sub-working group under the Building Collapse Simulation Working Group (WG) and the WG leader was Prof. Keiichiro Suita (Kyoto University, Japan). The authors acknowledge Dr. Bruce F. Maison (California, US), Prof. Satoshi Yamada (Tokyo Institute of Technology, Japan), Prof. Motohide Tada (Osaka University, Japan) and Dr. Yuko Shimada (Chiba University, Japan) for their enthusiastic technical support.

References

[1] Kasai K, Ooki Y, Motoyui S, Takeuchi T, Sato E (2007): E-Defense tests on full-scale steel buildings, part 1 - experiments using dampers and isolators. *Proceedings of Structural Congress*, ASCE, Long Beach, USA.
[2] Tada M, Ohsaki M, Yamada S, Motoyui S, Kasai K (2007): E-Defense tests on full-scale steel buildings, part 3 - analytical simulation of collapse. *Proceedings of Structural Congress*, ASCE, Long Beach, USA.
[3] Yamada S, Suita K, Tada M, Kasai K, Matsuoka Y, Shimada Y (2008): Collapse experiment on 4-story steel moment frame, part 1 – outline of test results. *14th World Conference on Earthquake Engineering*, Beijing, China.
[4] Suita K, Yamada S, Tada M, Kasai K, Matsuoka Y, Shimada Y (2008): Collapse experiment on 4-story steel moment frame, part 2 – detail of collapse behavior. *14th World Conference on Earthquake Engineering*, Beijing, China.
[5] Maison BF, Kasai K, Deierlein G (2009): ASCE-41 and FEMA-351 evaluation of E-Defense collapse test. *Earthquake Spectra,* **25** (4), 927–953.
[6] Lignos GD, Hikino T, Matsuoka Y, Nakashima M (2013): Collapse assessment of steel moment frames based on E-Defense full-scale shake table collapse test. *Journal of Structural Engineering*, **139**, 120–132.
[7] Tada M, Tamai H, Ohgami K, Kuwahara S, Horimoto A. Analytical simulation utilizing collaborative structural analysis system. *Proceedings of the 14th World Conference on Earthquake Engineering*, Beijing, 2008.
[8] Miyamura T, Yamashita T, Akiba H, Ohsaki M (2014): Dynamic FE simulation of four-story steel frame modeled by solid elements and its validation using results of full-scale shake-table test. *Earthquake Engineering & Structural Dynamics*, DOI: 10.1002/eqq.2526.
[9] Yu YJ, Tsai KC, Weng YT, Lin BZ, Lin JL (2010): Analytical studies of a full-scale steel building shaken to collapse. *Engineering Structures,* **32**, 3418–3430.
[10] Inoue I (2003): *Theory and design of steel structures* (in Japanese), Kyoto University Press.
[11] Yamada S, Ishida T, Shimada Y, Matsunaga T (2013): Cyclic loading test on RHS columns under bi-directional horizontal forces (in Japanese). *Journal of Structural and Construction Engineering, Transactions of AIJ*, **683**, 203–212.
[12] Yamada S, Akiyama H, Kuwamura H (1993): Post-buckling and deteriorating behavior of box-section steel members (in Japanese). *Journal of Structural and Construction Engineering, Transactions of AIJ*, **444**, 135–143.